

A numerical approximation method for the Fisher-Rao distance between multivariate normal distributions

Frank Nielsen
ORCID ID:0000-0001-5728-0726

Sony Computer Science Laboratories Inc, Tokyo, Japan.

Abstract

We present a simple method to approximate Rao's distance between multivariate normal distributions based on discretizing curves joining normal distributions and approximating Rao distances between successive nearby normal distributions on the curve by Jeffreys divergence. We consider experimentally the linear interpolation curves in the ordinary, natural and expectation parameterizations of the normal distributions, and compare these curves with a curve derived from the Calvo and Oller's isometric embedding of the Fisher-Rao d -variate normal manifold into the cone of $(d+1) \times (d+1)$ symmetric positive-definite matrices [Journal of multivariate analysis 35.2 (1990): 223-242]. We report on our experiments and assess the quality of our approximation technique by comparing the numerical approximations with lower and upper bounds. Finally, we present some information-geometric properties of the Calvo and Oller's isometric embedding.

Keywords: Fisher-Rao normal manifold; symmetric positive-definite matrix cone; isometric embedding; information geometry

1 Introduction

Let $\mathcal{P}(d)$ denote the set of symmetric positive-definite matrices (a convex regular cone), and $\mathcal{N}(d) = \{N(\mu, \Sigma) : (\mu, \Sigma) \in \mathbb{R}^d \times \mathcal{P}(d)\}$ denote the set of d -variate normal distributions (or Gaussians) with

$$N(\mu, \Sigma) \sim p_{\lambda=(\mu, \Sigma)}(x) = (2\pi)^{\frac{d}{2}} |\Sigma|^{-\frac{1}{2}} \exp\left(-\frac{1}{2}(x - \mu)^\top \Sigma^{-1}(x - \mu)\right), x \in \mathbb{R}^d.$$

The statistical model $\mathcal{N}(d)$ is of dimension $d + \frac{d(d+1)}{2} = \frac{d(d+3)}{2}$. By equipping $\mathcal{N}(d)$ with the Fisher information metric

$$g_{\mathcal{N}}^{\text{Fisher}}(\mu, \Sigma) = -E[\nabla^2 \log p_{(\mu, \Sigma)}(x)],$$

we get a Riemannian manifold called the Fisher-Rao Gaussian [38] with Riemannian geodesic distance $\rho_{\mathcal{N}}(\cdot, \cdot)$ called the Rao distance [3] or Fisher-Rao distance [36, 27, 10]. Historically, Hotelling [16] first used this distance in the late 1920's. From the viewpoint of information geometry [1], the Fisher metric is the unique Markov invariant metric up to rescaling [9, 5, 13] and the Fisher-Rao distance can be used in statistical hypothesis testing [6].

The squared line element $ds_{\mathcal{N}}^2(\mu, \Sigma) = g_{(\mu, \Sigma)}^{\text{Fisher}}(d\mu, d\Sigma)$ induced by the Fisher information metric of the normal family is

$$ds_{\mathcal{N}}^2(\mu, \Sigma) = d\mu^\top \Sigma^{-1} d\mu + \frac{1}{2} \text{tr} \left((\Sigma^{-1} d\Sigma)^2 \right).$$

In general, the Fisher-Rao distance between multivariate normal distributions is not known in closed-form [12, 17, 18], and several lower and upper bounds [39], and numerical techniques like geodesic shooting [15, 33, 4] have been investigated: See [34] for a review. The two difficulties to calculate the Fisher-Rao distance are (1) to know explicitly the expression of the Riemannian Fisher-Rao geodesic $\gamma_{\mathcal{N}}^{\text{FR}}$ and (2) to integrate in closed-form the length element $ds_{\mathcal{N}}$ along this Riemannian geodesic. Note that the Fisher-Rao geodesics $\gamma_{\mathcal{N}}^{\text{FR}}(t)$ are parameterized have constant speed (i.e., $\dot{\mu}(t) = \dot{\mu}(0)$ and $\dot{\Sigma}(t) = \dot{\Sigma}(0)$, proportional to arc length parameterization). However, in several special cases, the Fisher-Rao distance between normal distributions is known. Three such cases are (1) when the normal distributions are univariate ($d = 1$) and when the normal distributions belong to (2) some submanifold $\mathcal{N}_{\Sigma} = \{N(\mu, \Sigma) : \mu \in \mathbb{R} - d\} \subset \mathcal{N}$ of normal distributions sharing the same mean covariance matrix Σ , and (3) some submanifold $\mathcal{N}_{\mu} = \{N(\mu, \Sigma) : \Sigma \in \mathcal{P}(d)\} \subset \mathcal{N}$ of normal distributions sharing the same mean μ . In the first case, the Fisher-Rao distance between $N_1 = N(\mu_1, \sigma_1^2)$ and $N_2 = N(\mu_2, \sigma_2^2)$ can be derived from the hyperbolic distance expressed in the Poincaré upper space:

$$\rho_{\mathcal{N}}(N_1, N_2) = \sqrt{2} \log \frac{1 + \Delta(\mu_1, \sigma_1; \mu_2, \sigma_2)}{1 - \Delta(\mu_1, \sigma_1; \mu_2, \sigma_2)},$$

with

$$\Delta(a, b; c, d) = \sqrt{\frac{(c-a)^2 + 2(d-b)^2}{(c-a)^2 + 2(d+b)^2}}.$$

In the second case, the Rao distance between $N_1 = N(\mu_1, \Sigma)$ and $N_2 = N(\mu_2, \Sigma_1)$ amounts to Mahalanobis distance [3]:

$$\rho_{\mathcal{N}_{\mu}}(N_1, N_2) = \sqrt{(\mu_2 - \mu_1)^\top \Sigma^{-1} (\mu_2 - \mu_1)}.$$

In the third case, Rao distance between $N_1 = N(\mu, \Sigma_1)$ and $N_2 = N(\mu, \Sigma_2)$ has been reported in [19, 38] (see also [45]):

$$\rho_{\mathcal{N}_{\mu}}(N_1, N_2) = \sqrt{\frac{1}{2} \sum_{i=1}^d \log^2 \lambda_i(\Sigma_1^{-1} \Sigma_2)},$$

where $\lambda_i(M)$ denotes the i -th largest eigenvalue of matrix M . Let us notice that $\rho_{\mathcal{N}_{\mu}}((\mu, \Sigma_1), (\mu, \Sigma_2)) = \rho_{\mathcal{N}_{\mu}}((\mu, \Sigma_1^{-1}), (\mu, \Sigma_2^{-1}))$ since $\lambda_i(\Sigma_2^{-1} \Sigma_1) = \frac{1}{\lambda_i(\Sigma_1^{-1} \Sigma_2)}$ and $\log^2 \lambda_i(\Sigma_2^{-1} \Sigma_1) = (-\log \lambda_i(\Sigma_1^{-1} \Sigma_2))^2 = \log^2 \lambda_i(\Sigma_1^{-1} \Sigma_2)$.

In general, the difficulty of calculating the Fisher-Rao distance comes from the fact that (1) we do not know the Fisher-Rao geodesics with boundary value conditions in closed form (only the geodesics with initial value conditions [8] are known), (2) we have to integrate the line element $ds_{\mathcal{N}}$ along the geodesic. The lack of closed-form formula and fast and good approximations for $\rho_{\mathcal{N}}$ between normals is a current limiting factor for applications. The geometry of zero-centered generalized multivariate Gaussians was recently studied in [42].

The main contribution of this paper is to propose an approximation of $\rho_{\mathcal{N}}$ based on Calvo & Oller's embedding [6] and report its experimental performance. First, we concisely recall Calvo and

Oller's family of embeddings f_β of $\mathcal{N}(d)$ as submanifolds $\overline{\mathcal{N}}_\beta$ of $\mathcal{P}(d+1)$ in Section 2. Next, we present our approximation technique in Section 3 which differs from the usual geodesic shooting approach [15], and report experimental results. Finally, we study some information-geometric properties [1] of the isometric embedding in §4 like the fact that it preserves mixture but not exponential geodesics.

2 Calvo and Oller's family of embeddings

Calvo and Oller [6, 7] noticed that we can embed normal distributions in $\mathcal{P}(d+1)$ by the following mapping:

$$f_\beta(\mu, \Sigma) = \begin{bmatrix} \Sigma + \beta\mu\mu^\top & \beta\mu \\ \beta\mu^\top & \beta \end{bmatrix} \in \mathcal{P}(d+1), \quad (1)$$

where $\beta \in \mathbb{R}_{>0}$. Notice that since the dimension of $\mathcal{P}(d+1)$ is $\frac{(d+1)(d+2)}{2}$, we only use $\frac{(d+1)(d+2)}{2} - \frac{d(d+3)}{2} = 1$ extra dimension for embedding $\mathcal{N}(d)$ into $\mathcal{P}(d+1)$. Let

$$\overline{\mathcal{N}}_\beta(d) = \left\{ \bar{P} = f_\beta(\mu, \Sigma) : (\mu, \Sigma) \in \mathbb{R}^d \times \mathcal{P}(d) \right\}$$

denote the submanifold of $\mathcal{P}(d+1)$ of codimension 1, and $\overline{\mathcal{N}} = \overline{\mathcal{N}}_1$. The family of mappings f_β provides diffeomorphisms between $\mathcal{N}(d)$ and $\overline{\mathcal{N}}_\beta(d)$. Let $f_\beta^{-1}(\bar{P}) = (\mu_{\bar{P}}, \Sigma_{\bar{P}})$ denote the inverse mapping, and let $f = f_1$.

By equipping the cone $\mathcal{P}(d+1)$ by the trace metric [24]

$$g_P^{\text{trace}}(P_1, P_2) = \text{tr}(P^{-1}P_1P^{-1}P_2)$$

scaled by $\frac{1}{2}$ (yielding the squared line element $ds_P^2 = \frac{1}{2}\text{tr}((PdP)^2)$), Calvo and Oller [6] proved that $\overline{\mathcal{N}}(d)$ is isometric to $\mathcal{N}(d)$ (i.e., the Riemannian metric of $\mathcal{P}(d+1)$ restricted to $\mathcal{N}(d)$ coincides with the Riemannian metric of $\mathcal{N}(d)$ induced by f) but $\overline{\mathcal{N}}(d)$ is not totally geodesic (i.e., the geodesics $\gamma_{\mathcal{P}}(\bar{P}_1, \bar{P}_2; t)$ for $\bar{P}_1 = f(N_1), \bar{P}_2 = f(N_2) \in \overline{\mathcal{N}}(d)$ leaves the embedded normal submanifold $\overline{\mathcal{N}}(d)$). Note that the trace metric was first studied by Siegel [37, 29] using the wider scope of complex symmetric matrices with positive-definite imaginary parts generalizing the Poincaré upper half-plane (see Appendix A).

We omit to specify the dimensions and write for short \mathcal{N} , $\overline{\mathcal{N}}$ and \mathcal{P} when clear from context. Thus Calvo and Oller proposed to use the embedding $f = f_1$ to give a lower bound ρ_{CO} of the Fisher-Rao distance $\rho_{\mathcal{N}}$ between normals:

$$\rho_{\mathcal{N}}(N_1, N_2) \geq \rho_{\text{CO}}(\underbrace{f(\mu_1, \Sigma_1)}_{\bar{P}_1}, \underbrace{f(\mu_2, \Sigma_2)}_{\bar{P}_2}) = \sqrt{\frac{1}{2} \sum_{i=1}^{d+1} \log^2 \lambda_i(\bar{P}_1^{-1}\bar{P}_2)}.$$

The Calvo & Oller distance ρ_{CO} is a metric distance that has been used in many applications ranging from computer vision [43, 26] to signal/sensor processing, machine learning [40, 44, 20, 21, 32] and analogical reasoning [25].

Remark 1 In a second paper, Calvo and Oller [7] noticed that we can embed normal distributions in $\mathcal{P}(d+1)$ by the following mapping (Lemma 3.1 [7]):

$$g_{\alpha, \beta, \gamma}(\mu, \Sigma) = |\Sigma|^\alpha \begin{bmatrix} \Sigma + \beta\gamma^2\mu\mu^\top & \beta\gamma\mu \\ \beta\gamma\mu^\top & \beta \end{bmatrix} \in \mathcal{P}(d+1), \quad (2)$$

where $\alpha \in \mathbb{R}$, $\beta \in \mathbb{R}_{>0}$ and $\gamma \in \mathbb{R}$. In some applications [35], the embedding

$$g_{-\frac{1}{d+1}, 1, 1}(\mu, \Sigma) = |\Sigma|^{-\frac{1}{d+1}} \begin{bmatrix} \Sigma + \mu\mu^\top & \mu \\ \mu^\top & 1 \end{bmatrix}, \quad (3)$$

is used to ensure that $|g_{-\frac{1}{d+1}, 1, 1}(\mu, \Sigma)| = 1$. That is normal distributions are embedded diffeomorphically into the submanifold of positive-definite matrices with unit determinant (also called SSPD, acronym of Special SPD). The Gaussian manifold can be embedded in the SPD cone as a Riemannian symmetric space [22, 14] by the following mapping:

$$s(\mu, S) = |S|^{-\frac{2}{d+1}} \begin{bmatrix} SS^\top + \mu\mu^\top & \mu \\ \mu^\top & \beta \end{bmatrix} \in \mathcal{P}(d+1), \quad (4)$$

where $\Sigma = SS^\top$ is the decomposition of the covariance matrix $\Sigma \succ 0$ using the unique square root matrix: $S \in \mathrm{GL}(d)$.

3 Approximating the Fisher-Rao distance

3.1 Approximating length of curves on \mathcal{N}

Rao's distance [23] is a Riemannian geodesic distance

$$\rho_{\mathcal{N}}(p_{\lambda_1}, p_{\lambda_2}) = \inf_c \{\mathrm{Length}(c) : c(0) = p_{\lambda_1}, c(1) = p_{\lambda_2}\},$$

where

$$\mathrm{Length}(c) = \int_0^1 \underbrace{\sqrt{\langle \dot{c}(t), \dot{c}(t) \rangle_{c(t)}}}_{\mathrm{ds}_{\mathcal{N}}(t)} \mathrm{d}t.$$

Thus we can approximate the Rao distance $\rho_{\mathcal{N}}(N_1, N_2)$ by discretizing regularly any smooth curve $c(t)$ joining N_1 ($t = 0$) to N_2 ($t = 1$):

$$\rho_{\mathcal{N}}(N_1, N_2) \leq \frac{1}{T} \sum_{i=1}^{T-1} \rho_{\mathcal{N}} \left(c \left(\frac{i}{T} \right), c \left(\frac{i+1}{T} \right) \right),$$

with equality holding iff $c(t) = \gamma_{\mathcal{N}}(N_1, N_2; t)$ is the Riemannian geodesic induced by the Fisher information metric.

When T is sufficiently large, the normal distributions $c \left(\frac{i}{T} \right)$ and $c \left(\frac{i+1}{T} \right)$ are close to each other, and we can approximate $\rho_{\mathcal{N}} \left(c \left(\frac{i}{T} \right), c \left(\frac{i+1}{T} \right) \right)$ by $\sqrt{D_J \left[c \left(\frac{i}{T} \right), c \left(\frac{i+1}{T} \right) \right]}$, where $D_J[N_1, N_2] = D_{\mathrm{KL}}[N_1, N_2] + D_{\mathrm{KL}}[N_2, N_1]$ is Jeffreys divergence, and D_{KL} is the Kullback-Leibler divergence:

$$D_{\mathrm{KL}}[p_{(\mu_1, \Sigma_1)} : p_{(\mu_2, \Sigma_2)}] = \frac{1}{2} \left(\mathrm{tr}(\Sigma_2^{-1} \Sigma_1) + \Delta\mu^\top \Sigma_2^{-1} \Delta\mu - d + \log \frac{|\Sigma_2|}{|\Sigma_1|} \right).$$

Thus the costly determinant computations cancel each others in Jeffreys divergence (i.e., $\log \frac{|\Sigma_2|}{|\Sigma_1|} + \log \frac{|\Sigma_1|}{|\Sigma_2|} = 0$) and we have:

$$D_J[p_{(\mu_1, \Sigma_1)} : p_{(\mu_2, \Sigma_2)}] = \mathrm{tr} \left(\frac{\Sigma_2^{-1} \Sigma_1 + \Sigma_1^{-1} \Sigma_2}{2} - I \right) + \Delta\mu^\top \frac{\Sigma_1^{-1} + \Sigma_2^{-1}}{2} \Delta\mu.$$

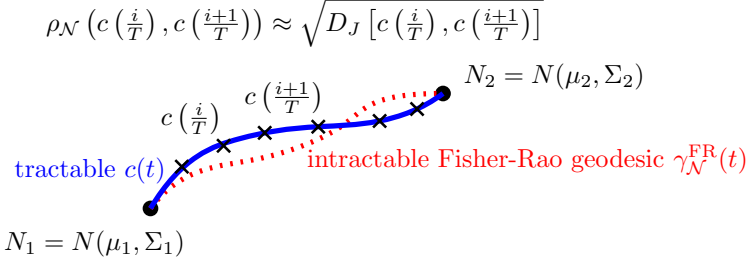


Figure 1: Approximating the Fisher-Rao geodesic distance $\rho_{\mathcal{N}}(N_1, N_2)$: The Fisher-Rao geodesic $\gamma_{\mathcal{N}}^{\text{FR}}$ is not known in closed-form. We consider a tractable curve $c(t)$, discretize $c(t)$ at $T+1$ points $c(\frac{i}{T})$ with $c(0) = N_1$ and $c(1) = N_2$, and approximate $\rho_{\mathcal{N}}(c(\frac{i}{T}), c(\frac{i+1}{T}))$ by $D_J[c(\frac{i}{T}), c(\frac{i+1}{T})]$. Considering different tractable curves $c(t)$ yield different approximations.

Figure 1 summarizes our method to approximate the Fisher-Rao geodesic distance.

In general, it holds that $I_f[p : q] \approx \frac{f''(1)}{2} ds_{\text{Fisher}}^2$ between infinitesimally close distributions p and q ($ds \approx \sqrt{\frac{2I_f[p:q]}{f''(1)}}$), where I_f denotes a f -divergence [1]. The Jeffreys divergence is a f -divergence obtained for $f_J(u) = -\log u + u \log u$ with $f_J''(1) = 2$.

Although the definite integral of the length element along the Fisher-Rao geodesic $\gamma_{\mathcal{N}}^{\text{FR}}$ is not known in closed form (i.e., Fisher-Rao distance), the integral of the squared length element along the mixture geodesic $\gamma_{\mathcal{N}}^m$ and exponential geodesic $\gamma_{\mathcal{N}}^e$ coincide with Jeffreys divergence [1]:

Property 1 ([1]) *We have*

$$D_J[p_{\lambda_1}, p_{\lambda_2}] = \int_0^1 ds_{\mathcal{N}}^2(\gamma_{\mathcal{N}}^m(p_{\lambda_1}, p_{\lambda_2}; t) dt = \int_0^1 ds_{\mathcal{N}}^2(\gamma_{\mathcal{N}}^e(p_{\lambda_1}, p_{\lambda_2}; t) dt.$$

Proof: Let us report a proof of this remarkable fact in the general setting of Bregman manifolds (proof omitted in [1]). Since $D_J[p_{\lambda_1}, p_{\lambda_2}] = D_{\text{KL}}[p_{\lambda_1}, p_{\lambda_2}] + D_{\text{KL}}[p_{\lambda_2}, p_{\lambda_1}]$ and $D_{\text{KL}}[p_{\lambda_1}, p_{\lambda_2}] = B_F(\theta(\lambda_2) : \theta(\lambda_1))$, where B_F denotes the Bregman divergence induced by the cumulant function of the multivariate normals and $\theta(\lambda)$ is the natural parameter corresponding to λ , we have

$$\begin{aligned} D_J[p_{\lambda_1}, p_{\lambda_2}] &= B_F(\theta_1 : \theta_2) + B_F(\theta_2 : \theta_1), \\ &= S_F(\theta_1; \theta_2) = (\theta_2 - \theta_1)^\top (\eta_2 - \eta_1) = S_{F^*}(\eta_1; \eta_2), \end{aligned}$$

where $\eta = \nabla F(\theta)$ and $\theta = \nabla F^*(\eta)$ denote the dual parameterizations obtained by the Legendre-Fenchel convex conjugate $F^*(\eta)$ of $F(\theta)$. The proof is based on the first-order and second-order directional derivatives. The first-order directional derivative $\nabla_u F(\theta)$ with respect to vector u is defined by

$$\nabla_u F(\theta) = \lim_{t \rightarrow 0} \frac{F(\theta + tv) - F(\theta)}{t} = v^\top \nabla F(\theta).$$

The second-order directional derivatives $\nabla_{u,v}^2 F(\theta)$ is

$$\begin{aligned} \nabla_{u,v}^2 F(\theta) &= \nabla_u \nabla_v F(\theta), \\ &= \lim_{t \rightarrow 0} \frac{v^\top \nabla F(\theta + tu) - v^\top \nabla F(\theta)}{t}, \\ &= u^\top \nabla^2 F(\theta) v. \end{aligned}$$

Now consider the squared length element $ds^2(\gamma(t))$ on the primal geodesic $\gamma(t)$ expressed using the primal coordinate system θ : $ds^2(\gamma(t)) = d\theta(t)^\top \nabla^2 F(\theta(t)) d\theta(t)$ with $\theta(\gamma(t)) = \theta_1 + t(\theta_2 - \theta_1)$ and $d\theta(t) = \theta_2 - \theta_1$. Let us express the $ds^2(\gamma(t))$ using the second-order directional derivative:

$$ds^2(\gamma(t)) = \nabla_{\theta_2 - \theta_1}^2 F(\theta(t)).$$

Thus we have $\int_0^1 ds^2(\gamma(t)) dt = [\nabla_{\theta_2 - \theta_1} F(\theta(t))]_0^1$, where the first-order directional derivative is $\nabla_{\theta_2 - \theta_1} F(\theta(t)) = (\theta_2 - \theta_1)^\top \nabla F(\theta(t))$. Therefore we get $\int_0^1 ds^2(\gamma(t)) dt = (\theta_2 - \theta_1)^\top (\nabla F(\theta_2) - \nabla F(\theta_1)) = S_F(\theta_1; \theta_2)$.

Similarly, we express the squared length element $ds^2(\gamma^*(t))$ using the dual coordinate system η as the second-order directional derivative of $F^*(\eta(t))$ with $\eta(\gamma^*(t)) = \eta_1 + t(\eta_2 - \eta_1)$:

$$ds^2(\gamma^*(t)) = \nabla_{\eta_2 - \eta_1}^2 F^*(\eta(t)).$$

Therefore, we have $\int_0^1 ds^2(\gamma^*(t)) dt = [\nabla_{\eta_2 - \eta_1} F^*(\eta(t))]_0^1 = S_{F^*}(\eta_1; \eta_2)$. Since $S_{F^*}(\eta_1; \eta_2) = S_F(\theta_1; \theta_2)$, we conclude that

$$S_F(\theta_1; \theta_2) = \int_0^1 ds^2(\gamma(t)) dt = \int_0^1 ds^2(\gamma^*(t)) dt$$

In 1D, both pregeodesics $\gamma(t)$ and $\gamma^*(t)$ coincide. We have $ds^2(t) = (\theta_2 - \theta_1)^2 f''(\theta(t)) = (\eta_2 - \eta_1) f''(\eta(t))$ so that we check that $S_F(\theta_1; \theta_2) = \int_0^1 ds^2(\gamma(t)) dt = (\theta_2 - \theta_1) [f'(\theta(t))]_0^1 = (\eta_2 - \eta_1) [f'^*(\eta(t))]_0^1 = (\eta_2 - \eta_1)(\theta_2 - \theta_1)$. \square

It follows the following property:

Property 2 (Fisher-Rao upper bound) *The Fisher-Rao distance between normal distributions is upper bounded by the square root of the Jeffreys divergence: $\rho_N(N_1, N_2) \leq \sqrt{D_J(N_1, N_2)}$.*

Proof: Consider the Cauchy-Schwarz inequality for positive functions $f(t)$ and $g(t)$: $\int_0^1 f(t)g(t) dt \leq \sqrt{(\int_0^1 f(t)^2 dt)(\int_0^1 g(t)^2 dt)}$, and let $f(t) = ds_N(\gamma_N^c(p_{\lambda_1}, p_{\lambda_2}; t))$ and $g(t) = 1$. Then we get:

$$\left(\int_0^1 ds_N(\gamma_N^c(p_{\lambda_1}, p_{\lambda_2}; t)) dt \right)^2 \leq \left(\int_0^1 ds_N^2(\gamma_N^c(p_{\lambda_1}, p_{\lambda_2}; t)) dt \right) \left(\int_0^1 1^2 dt \right)$$

Furthermore since by definition of γ_N^{FR} , we have $\int_0^1 ds_N(\gamma_N^c(p_{\lambda_1}, p_{\lambda_2}; t)) dt \geq \int_0^1 ds_N(\gamma_N^{\text{FR}}(p_{\lambda_1}, p_{\lambda_2}; t)) dt =: \rho_N(N_1, N_2)$, it follows for $c = e$ (i.e., e -geodesic γ_N^e), we have:

$$\rho_N(N_1, N_2)^2 \leq \int_0^1 ds_N^2(\gamma_N^e(p_{\lambda_1}, p_{\lambda_2}; t)) dt = D_J(N_1, N_2).$$

Thus we have $\rho_N(N_1, N_2) \leq \sqrt{D_J(N_1, N_2)}$.

Note that in Riemannian geometry, a curve γ minimizes the energy $E(\gamma) = \int_0^1 |\dot{\gamma}(t)|^2 dt$ if it minimizes the length $L(\gamma) = \int_0^1 \|\dot{\gamma}(t)\| dt$ and $\|\dot{\gamma}(t)\|$ is constant. Using Cauchy-Schwartz inequality, we can show that $L(\gamma) \leq E(\gamma)$. \square

Note that this upper bound is tight at infinitesimal scale (i.e., when $N_2 = N_1 + dN$).

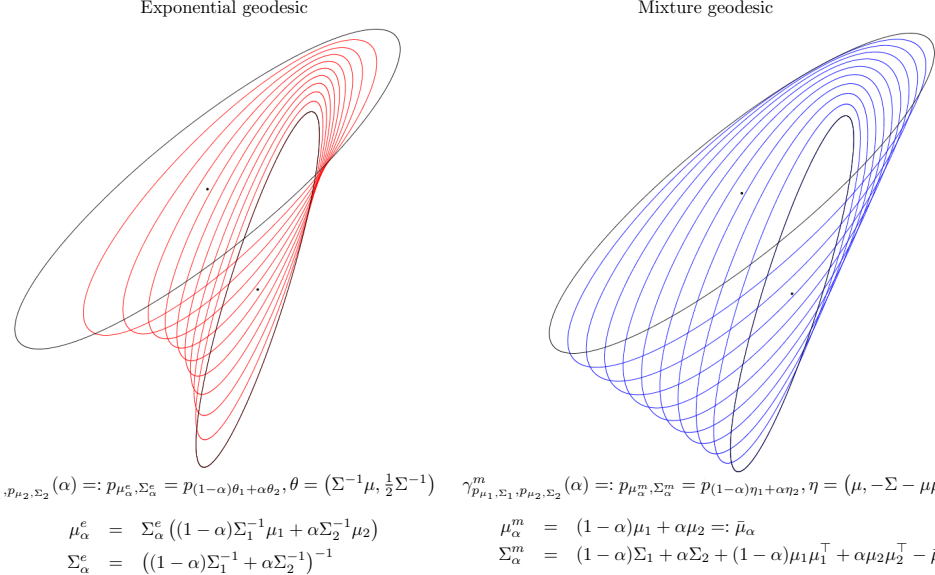


Figure 2: Visualizing the exponential and mixture geodesics between two bivariate normal distributions.

For any smooth curve $c(t)$, we thus approximate $\rho_{\mathcal{N}}$ by

$$\tilde{\rho}_{\mathcal{N}}^c(N_1, N_2) := \frac{1}{T} \sum_{i=1}^{T-1} \sqrt{D_J \left[c \left(\frac{i}{T} \right), c \left(\frac{i+1}{T} \right) \right]}.$$

(5)

For example, we may consider the following curves on \mathcal{N} which admit closed-form parameterizations in $t \in [0, 1]$:

- linear interpolation $c_\lambda(t) = t(\mu_1, \Sigma_1) + (1-t)(\mu_2, \Sigma_2)$ between (μ_1, Σ_1) and (μ_2, Σ_2) ,
- the mixture geodesic [28] $c_m(t) = \gamma_{\mathcal{N}}^m(N_1, N_2; t) = (\mu_t^m, \Sigma_t^m)$ with $\mu_t^m = \bar{\mu}_t$ and $\Sigma_t^m = \bar{\Sigma}_t + t\mu_1\mu_1^\top + (1-t)\mu_2\mu_2^\top - \bar{\mu}_t\bar{\mu}_t^\top$ where $\bar{\mu}_t = t\mu_1 + (1-t)\mu_2$ and $\bar{\Sigma}_t = t\Sigma_1 + (1-t)\Sigma_2$,
- the exponential geodesic [28] $c_e(t) = \gamma_{\mathcal{N}}^e(N_1, N_2; t) = (\mu_t^e, \Sigma_t^e)$ with $\mu_t^e = \bar{\Sigma}_t^H(t\Sigma_1^{-1}\mu_1 + (1-t)\Sigma_2^{-1}\mu_2)$ and $\Sigma_t^e = \bar{\Sigma}_t^H$ where $\bar{\Sigma}_t^H = (t\Sigma_1^{-1} + (1-t)\Sigma_2^{-1})^{-1}$ is the matrix harmonic mean,
- the curve $c_{em}(t) = \frac{1}{2}(\gamma_{\mathcal{N}}^e(N_1, N_2; t) + \gamma_{\mathcal{N}}^m(N_1, N_2; t))$ which is obtained by averaging the mixture geodesic with the exponential geodesic.

Let us denote by $\tilde{\rho}_{\mathcal{N}}^\lambda = \tilde{\rho}_{\mathcal{N}}^{c_\lambda}$, $\tilde{\rho}_{\mathcal{N}}^m = \tilde{\rho}_{\mathcal{N}}^{c_m}$, $\tilde{\rho}_{\mathcal{N}}^e = \tilde{\rho}_{\mathcal{N}}^{c_e}$ and $\tilde{\rho}_{\mathcal{N}}^{em} = \tilde{\rho}_{\mathcal{N}}^{c_{em}}$ the approximations obtained by these curves following from Eq. 5. Figure 2 visualizes the exponential and mixture geodesics between two bivariate normal distributions.

Note that we consider the regular spacing for approximating a curve length and do not optimize the position of the sample points on the curve. Indeed, as $T \rightarrow \infty$, the curve length approximation tends to the Riemannian curve length. In other words, we can measure approximately finely the length of any curve available with closed-form reparameterization by increasing T . Thus the key question of our method is how to best approximate the Fisher-Rao geodesic by a closed-form curve.

Remark 2 In [14], the authors consider the embedding of Eq. 4 and use the Killing metric g^{Killing} instead of the Fisher metric defined by:

$$g_N^{\text{Killing}}(N_1, N_2) = \mu_1^\top \Sigma^{-1} \mu_2 + \frac{1}{2} \text{tr}(\Sigma^{-1} \Sigma_1 \Sigma^{-1} \Sigma_2) - \frac{1}{2(d+1)} \text{tr}(\Sigma^{-1} \Sigma_1) \text{tr}(\Sigma^{-1} \Sigma_2),$$

where $N = (\mu, \Sigma)$, $N_1 = (\mu_1, \Sigma_1)$, and $N_2 = (\mu_2, \Sigma_2)$. A Fisher geodesic defect measure of a curve c is defined by

$$\delta(c) = \lim_{s \rightarrow \infty} \frac{1}{s} \int_0^s \|\nabla_{\dot{c}}^{g^{\text{Fisher}}} \dot{c}\|_{c(t)}^{\text{Fisher}} dt,$$

where $\nabla^{g^{\text{Fisher}}}$ denotes the Levi-Civita connection induced by the Fisher metric. When $\delta(c) = 0$ the curve is said an asymptotic geodesic of the Fisher geodesic. It is proven that Killing geodesics at (μ, Σ) are asymptotic Fisher geodesics when the initial condition $c'(0)$ is orthogonal to \mathcal{N}_μ .

Next, we introduce yet another curve $c_{\text{CO}}(t)$ derived from Calvo & Oller isometric mapping f which experimentally behaves better when normals are not *too far* from each others.

3.2 Calvo & Oller's curve

This approximation consists in leveraging the closed-form expression of the SPD geodesics [24, 2]:

$$\gamma_{\mathcal{P}}(P, Q; t) = P^{\frac{1}{2}} \left(P^{-\frac{1}{2}} Q^{\frac{1}{2}} P^{-\frac{1}{2}} \right)^t P^{\frac{1}{2}},$$

to approximate the Fisher-Rao normal geodesic $\gamma_{\mathcal{N}}(N_1, N_2; t)$ as follows: Let $\bar{P}_1 = f(N_1), \bar{P}_2 = f(N_2) \in \bar{\mathcal{N}}$, and consider the smooth curve

$$\bar{c}_{\text{CO}}(P_1, P_2; t) = \text{proj}_{\bar{\mathcal{N}}}(\gamma_{\mathcal{P}}(\bar{P}_1, \bar{P}_2; t)),$$

where $\text{proj}_{\bar{\mathcal{N}}}(P)$ denotes the Fisher orthogonal projection of $P \in \mathcal{P}(d+1)$ onto $\bar{\mathcal{N}}$ (Figure 4). Thus curve c_{CO} is then defined as $f^{-1}(\bar{c}_{\text{CO}})$. Note that the power matrix P^t is $U \text{diag}(\lambda_1^t, \dots, \lambda_d^t) V^\top$ where $P = U \text{diag}(\lambda_1^t, \dots, \lambda_d^t) V^\top$ is the eigenvalue decomposition of P .

Let us now explain how to project $P = [P_{i,j}] \in \mathcal{P}(d+1)$ onto $\bar{\mathcal{N}}$ based on the analysis of the Appendix of [6] (page 239):

Proposition 1 (Projection of a SPD matrix onto the embedded normal submanifold $\bar{\mathcal{N}}$)

Let $\beta = P_{d+1,d+1}$ and write $P = \begin{bmatrix} \Sigma + \beta \mu \mu^\top & \beta \mu \\ \beta \mu^\top & \beta \end{bmatrix}$. Then the orthogonal projection at $P \in \mathcal{P}$ onto $\bar{\mathcal{N}}$ is:

$$\bar{P}_\perp = \text{proj}_{\bar{\mathcal{N}}}(P) = \begin{bmatrix} \Sigma + \mu \mu^\top & \mu^\top \\ \mu & 1 \end{bmatrix},$$

and the SPD distance between P and \bar{P}_\perp is $\rho_{\mathcal{P}}(P, \bar{P}_\perp) = \frac{1}{\sqrt{2}} |\log \beta|$.

Note that the introduction of parameter β is related to the foliation of the SPD cone \mathcal{P} by $\{f_\beta(\mathcal{N}) : \beta > 0\}$: $\mathcal{P}(d+1) = \mathbb{R}_{>0} \times f_\beta(\mathcal{N})$. See Figure 3.

Let $\bar{c}_{\text{CO}}(t) = \bar{S}_t$ and $c_{\text{CO}}(t) = f^{-1}(\bar{c}_{\text{CO}}(t)) =: G_t$. The following proposition shows that we have $D_J[\bar{S}_t, \bar{S}_{t+1}] = D_J[G_t, G_{t+1}]$.

Proposition 2 The Kullback-Leibler divergence between p_{μ_1, Σ_1} and p_{μ_2, Σ_2} amounts to the KLD between $q_{\bar{P}_1} = p_{0, f(\mu_1, \Sigma_1)}$ and $q_{\bar{P}_2} = p_{0, f(\mu_2, \Sigma_2)}$ where $\bar{P}_i = f(\mu_i, \Sigma_i)$:

$$D_{\text{KL}}[p_{\mu_1, \Sigma_1} : p_{\mu_2, \Sigma_2}] = D_{\text{KL}}[q_{\bar{P}_1} : q_{\bar{P}_2}].$$

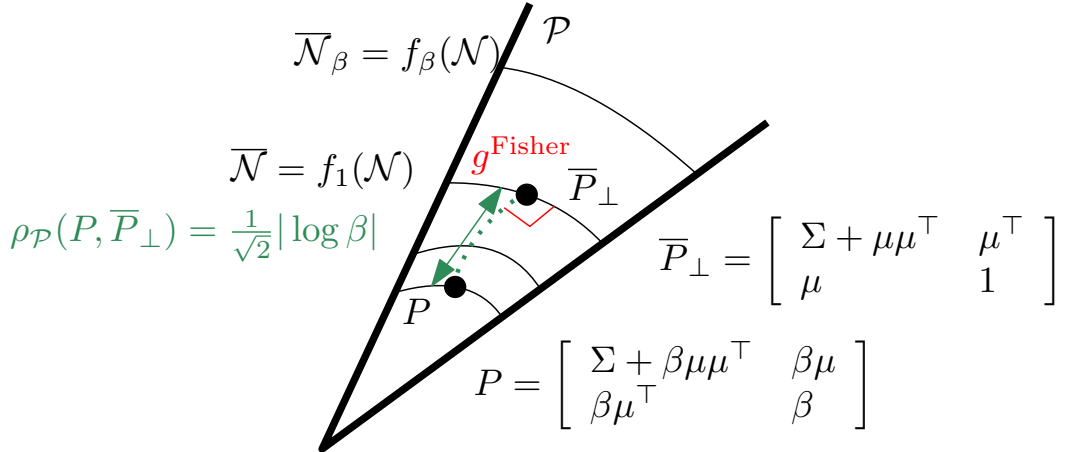


Figure 3: Projecting a SPD matrix $P \in \mathcal{P}$ onto $\overline{\mathcal{N}} = f(\mathcal{N})$.

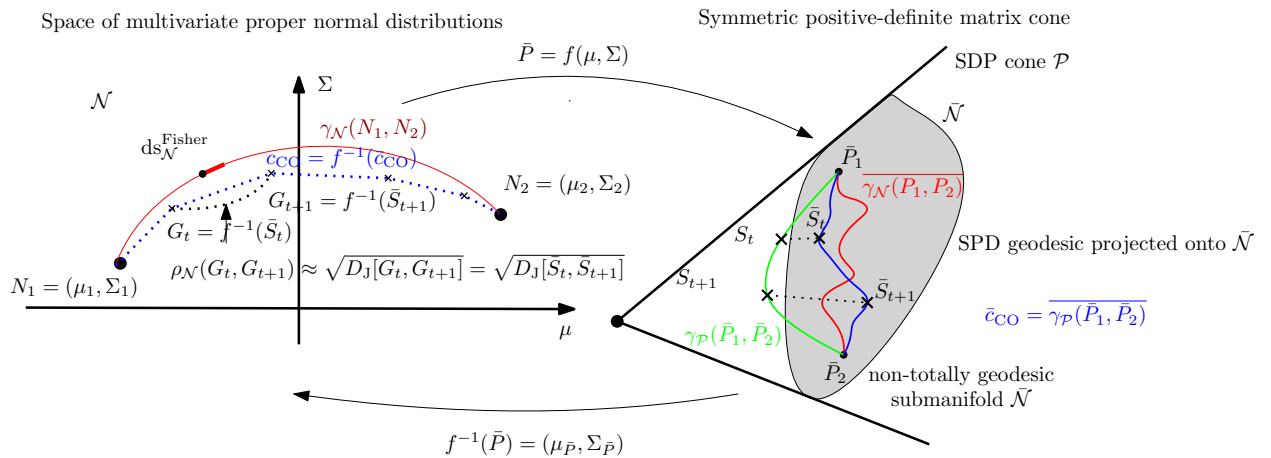


Figure 4: Illustration of the approximation of the Fisher-Rao distance between two normals N_1 and N_2 (red geodesic length $\gamma_{\mathcal{N}}(N_1, N_2)$) by discretizing $\bar{c}_{\text{CO}} \in \overline{\mathcal{N}}$ or equivalently $c_{\text{CO}} \in \mathcal{N}$.

Proof: The KLD between two centered $(d + 1)$ -variate normals $q_{P_1} = p_{0, P_1}$ and $q_{P_2} = p_{0, P_2}$ is

$$D_{\text{KL}}[q_{P_1} : q_{P_2}] = \frac{1}{2} \left(\text{tr}(P_2^{-1} P_1) - d - 1 + \log \frac{|P_2|}{|P_1|} \right).$$

This divergence can be interpreted as the matrix version of the Itakura-Saito divergence [11]. The SPD cone equipped with $\frac{1}{2}$ of the trace metric can be interpreted as Fisher-Rao centered normal manifolds: $(\mathcal{N}_\mu, g_{\mathcal{N}_\mu}^{\text{Fisher}}) = (\mathcal{P}, \frac{1}{2} g^{\text{trace}})$.

Since the determinant of a block matrix is

$$\left| \begin{bmatrix} A & B \\ C & D \end{bmatrix} \right| = |A - BD^{-1}C|,$$

we get with $D = 1$: $|f(\mu, \Sigma)| = |\Sigma + \mu\mu^\top - \mu\mu^\top| = |\Sigma|$.

Let $\bar{P}_1 = f(\mu_1, \Sigma_1)$ and $\bar{P}_2 = f(\mu_2, \Sigma_2)$. Checking $D_{\text{KL}}[p_{\mu_1, \Sigma_1} : p_{\mu_2, \Sigma_2}] = D_{\text{KL}}[q_{\bar{P}_1} : q_{\bar{P}_2}]$ where $q_{\bar{P}} = p_{0, \bar{P}}$ amounts to verify that

$$\text{tr}(\bar{P}_2^{-1} \bar{P}_1) = 1 + \text{tr}(\Sigma_2^{-1} \Sigma_1 + \Delta_\mu^\top \Sigma_2^{-1} \Delta_\mu).$$

Indeed, using the inverse matrix

$$f(\mu, \Sigma)^{-1} = \begin{bmatrix} \Sigma^{-1} & -\Sigma^{-1}\mu \\ -\mu^\top \Sigma^{-1} & 1 + \mu^\top \Sigma^{-1} \mu \end{bmatrix},$$

we have $\text{tr}(\bar{P}_2^{-1} \bar{P}_1) = \text{tr} \left(\begin{bmatrix} \Sigma_2^{-1} & -\Sigma_2^{-1}\mu_2 \\ -\mu_2^\top \Sigma_2^{-1} & 1 + \mu_2^\top \Sigma_2^{-1} \mu_2 \end{bmatrix} \begin{bmatrix} \Sigma_1 + \mu_1 \mu_1^\top & \mu_1 \\ \mu_1^\top & 1 \end{bmatrix} \right) = 1 + \text{tr}(\Sigma_2^{-1} \Sigma_1 + \Delta_\mu^\top \Sigma_2^{-1} \Delta_\mu)$. Thus even if the dimension of the sample spaces of $p_{\mu, \Sigma}$ and $q_{\bar{P} = f(\mu, \Sigma)}$ differs by one, we get the same KLD by Calvo and Oller's isometric mapping f . \square

This property holds for the KLD/Jeffreys divergence but not for all f -divergences [1] I_f in general (e.g., it fails for the Hellinger divergence).

Figure 5 shows the various geodesics and curves used to approximate the Fisher-Rao distance with the Fisher metric shown using Tissot indicatrices.

3.3 Some experiments

The KLD D_{KL} and Jeffreys divergence D_J , the Fisher-Rao distance $\rho_{\mathcal{N}}$ and the Calvo & Oller distance ρ_{CO} are all invariant under the congruence action of the affine group $\text{Aff}(d) = \mathbb{R}^d \rtimes \text{GL}(d)$ with group operation

$$(a_1, A_1)(a_2, A_2) = (a_1 + A_1 a_2, A_1 A_2).$$

Let $(A, a) \in \text{Aff}(d)$, and define the action on the normal space \mathcal{N} as follows:

$$(A, a).N(\mu, \Sigma) = N(A^\top \mu + a, A\Sigma A^\top).$$

Then we have $\rho_{\mathcal{N}}((A, a).N_1, (A, a).N_2) = \rho_{\mathcal{N}}(N_1, N_2)$, $\rho_{\text{CO}}((A, a).N_1, (A, a).N_2) = \rho_{\text{CO}}(N_1, N_2)$ and $D_{\text{KL}}[(A, a).N_1 : (A, a).N_2] = D_{\text{KL}}[N_1 : N_2]$. This invariance extends to our approximations $\tilde{\rho}_{\mathcal{N}}^c$ (see Eq. 5).

Since we have

$$\tilde{\rho}_{\mathcal{N}}^c(N_1, N_2) \approx \rho_{\mathcal{N}}(N_1, N_2) \geq \rho_{\text{CO}}(N_1, N_2),$$

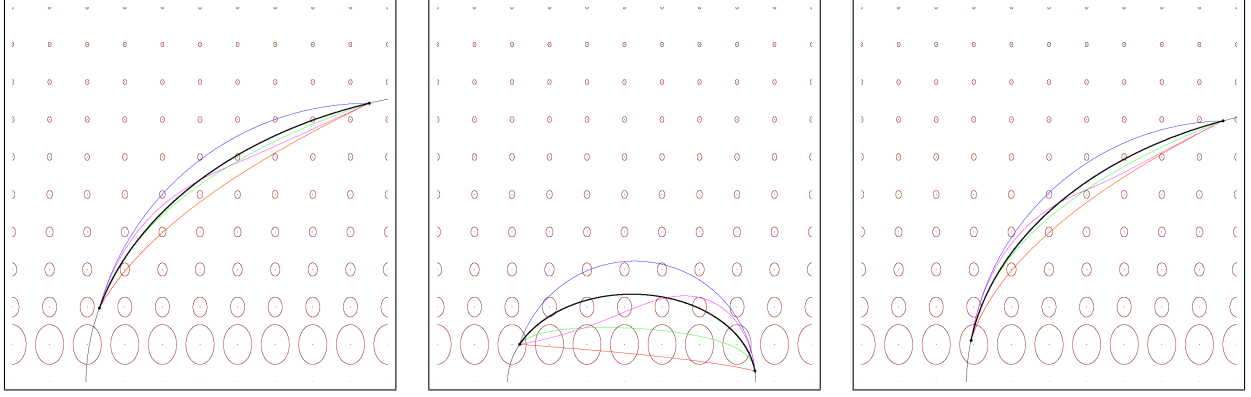


Figure 5: Geodesics and curves used to approximate the Fisher-Rao distance with the Fisher metric shown using Tissot’s indicatrices: exponential geodesic (red), mixture geodesic (blue), mid exponential-mixture curve (purple), projected CO curve (green) and target Fisher-Rao geodesic (black).

Table 1: First set of experiments demonstrates the advantage of the $c_{\text{CO}}(t)$ curve.

d	κ_{CO}	κ_l	κ_e	κ_m	κ_{em}
1	1.0025	1.0414	1.1521	1.0236	1.0154
2	1.0167	1.0841	1.1923	1.0631	1.0416
3	1.0182	1.8997	2.6072	1.9965	1.07988
4	1.0207	2.0793	1.8080	2.1687	1.1873
5	1.0324	4.1207	12.3804	5.6170	4.2349

the ratio $\kappa_c = \frac{\tilde{\rho}_{\mathcal{N}}^c}{\rho_{\text{CO}}} \geq \kappa = \frac{\tilde{\rho}_{\mathcal{N}}^c}{\rho_{\mathcal{N}}}$ gives an upper bound on the approximation factor of $\tilde{\rho}_{\mathcal{N}}^c$ compared to the true Fisher-Rao distance $\rho_{\mathcal{N}}$:

$$\kappa_c \rho_{\mathcal{N}}(N_1, N_2) \geq \kappa \rho_{\mathcal{N}}(N_1, N_2) \geq \tilde{\rho}_{\mathcal{N}}^c(N_1, N_2) \approx \rho_{\mathcal{N}}(N_1, N_2) \geq \rho_{\text{CO}}(N_1, N_2).$$

Let us now report some numerical experiments of our approximated Fisher-Rao distances $\tilde{\rho}_{\mathcal{N}}^x$ with $x \in \{l, m, e, \text{em}, \text{CO}\}$. When normal distributions are in 1D we can exactly plot the Fisher-Rao geodesics are locate the other geodesics/curves with respect to the Fisher-Rao geodesics (Figure 6). Although that dissimilarity $\tilde{\rho}_{\mathcal{N}}$ is positive-definite, it does not satisfy the triangular inequality of metric distances (e.g., Riemannian distances $\rho_{\mathcal{N}}$ and ρ_{CO}).

First, we draw multivariate normals by sampling means $\mu \sim \text{Unif}(0, 1)$ and sample covariance matrices Σ as follows: We draw a lower triangular matrix L with entries L_{ij} iid sampled from $\text{Unif}(0, 1)$, and take $\Sigma = LL^\top$. We use $T = 1000$ samples on curves and repeat the experiment 1000 times to gather average statistics on κ_c ’s of curves. Results are summarized in Table 1.

For that scenario that the C&O curve (either $\bar{c}_{\text{CO}} \in \overline{\mathcal{N}}$ or $c_{\text{CO}} \in \mathcal{N}$) performs best compared to the linear interpolation curves with respect to source parameter (l), mixture geodesic (m), exponential geodesic (e), or exponential-mixture mid curve (em). Let us point out that we sample $\gamma_{\mathcal{P}}(\bar{P}_1, \bar{P}_2; \frac{i}{T})$ for $i \in \{0, \dots, T\}$.

Strapasson, Porto and Costa [39] (SPC) reported the following upper bound on the Fisher-Rao

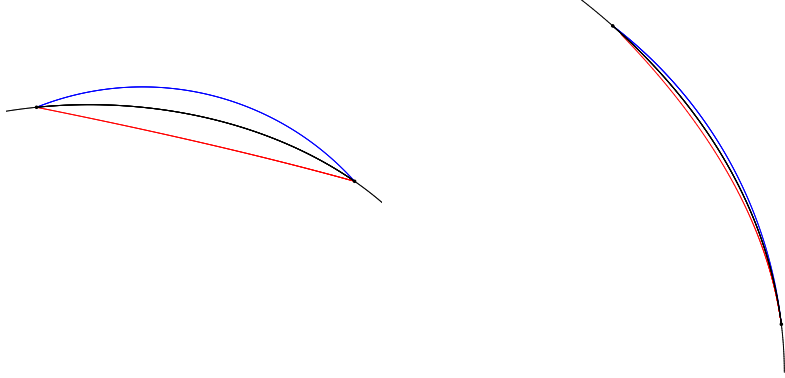


Figure 6: The full Fisher-Rao geodesic is shown in grey with the geodesic arc linking two univariate normal distributions shown in black. The exponential geodesics are shown in red and are below the Fisher-Rao geodesic. The mixture geodesics are shown in blue and are above the Fisher-Rao geodesic.

Table 2: Comparing our Fisher-Rao approximation with the Calvo & Oller lower bound and the Strapasson et al. upper bound.

d	$\rho_{\text{CO}}(N_1, N_2)$	$\tilde{\rho}^{\text{cCO}}(N_1, N_2)$	$U(N_1, N_2)$
1	1.7563	1.8020	3.1654
2	3.2213	3.3194	6.012
3	4.6022	4.7642	8.7204
4	5.9517	6.1927	11.3990
5	7.156	7.3866	13.8774

distance between multivariate normals:

$$\rho_{\text{CO}}(N_1, N_2) \leq \rho_{\mathcal{N}}(N_1, N_2) \leq U_{\text{SPC}}(N_1, N_2) = \sqrt{2 \sum_{i=1}^d \log^2 \left(\frac{\sqrt{(1+D_{ii})^2 + \mu_i^2} + \sqrt{(1-D_{ii})^2 + \mu_i^2}}{\sqrt{(1+D_{ii})^2 + \mu_i^2} - \sqrt{(1-D_{ii})^2 + \mu_i^2}} \right)}, \quad (6)$$

where $\Sigma = \Sigma_1^{-\frac{1}{2}} \Sigma_2 \Sigma_1^{-\frac{1}{2}}$, $\Sigma = \Omega D \Omega^\top$ is the eigen decomposition, and $\mu = \Omega^\top \Sigma_1^{-\frac{1}{2}} (\mu_2 - \mu_1)$. This upper bound performs better when the normals are well-separated and worse then the $\sqrt{D_J}$ -upper bound when the normals are close to each others.

Let us compare $\rho_{\text{CO}}(N_1, N_2)$ with $\rho_{\mathcal{N}}(N_1, N_2) \approx \tilde{\rho}^{\text{cCO}}(N_1, N_2)$ and the upper bound $U(N_1, N_2)$ by averaging over 1000 trials with N_1 and N_2 chosen randomly as before and $T = 1000$. We have $\rho_{\text{CO}}(N_1, N_2) \leq \rho_{\mathcal{N}}(N_1, N_2) \approx \tilde{\rho}^{\text{cCO}}(N_1, N_2) \leq U(N_1, N_2)$. Table 2 shows that our Fisher-Rao approximation is close to the lower bound (and hence to the underlying true Fisher-Rao distance) and that the upper bound is about twice the lower bound for that particular scenario.

The Fisher-Rao geodesics $\gamma_{\mathcal{N}}^{\text{FR}}(N_1, N_2)$ on the Fisher-Rao univariate normal manifolds are either vertical line segments when $\mu_1 = \mu_2$, or semi-circle with origin on the x -axis and x -axis stretched by $\sqrt{2}$ [41]:

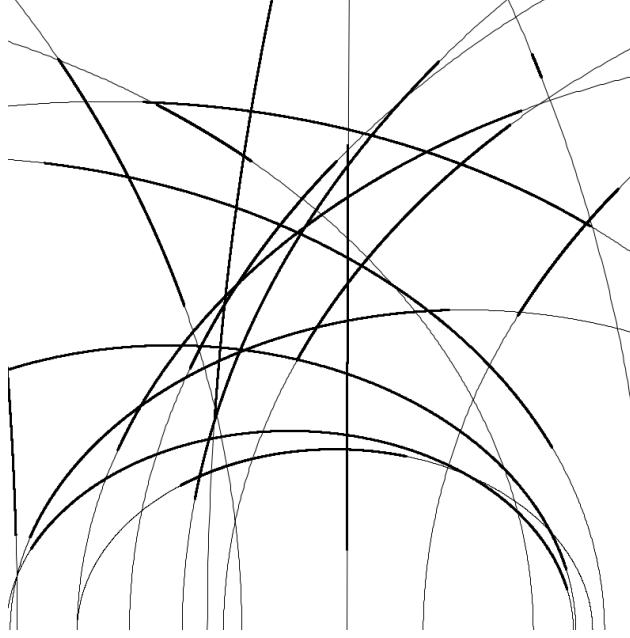


Figure 7: Visualizing some Fisher-Rao geodesics of univariate normal distributions on the Poincaré upper plane (semi-circles with origin on the x -axis and stretched by $\sqrt{2}$ on the x -axis). Full geodesics plotted with thin style and geodesic arcs plotted with thick style.

$$\gamma_N^{\text{FR}}(\mu_1, \sigma_1; \mu_2, \sigma_2) = \begin{cases} (\mu, (1-t)\sigma_1 + t\sigma_2), & \mu_1 = \mu_2 = \mu \\ (\sqrt{2}(c + r \cos t, r \sin t), t \in [\min\{\theta_1, \theta_2\}, \max\{\theta_1, \theta_2\}]), & \mu_1 \neq \mu_2, \end{cases},$$

where

$$c = \frac{\frac{1}{2}(\mu_2^2 - \mu_1^2) + \sigma_2^2 - \sigma_1^2}{\sqrt{2}(\mu_1 - \mu_2)}, \quad r = \sqrt{\left(\frac{\mu_i}{\sqrt{2}} - c\right)^2 + \sigma_i^2}, \quad i \in \{1, 2\},$$

and

$$\theta_i = \arctan\left(\frac{\sigma_i}{\frac{\mu_i}{\sqrt{2}} - c}\right), \quad i \in \{1, 2\},$$

provided that $\theta_i \geq 0$ for $i \in \{1, 2\}$ (otherwise, we let $\theta_i \leftarrow \theta_i + \pi$). Figure 7 displays some geodesics on the Fisher-Rao univariate normal manifold. Figure 8 displays the considered geodesics and curves in the stretched Poincaré upper plane of univariate normal distributions (x -axis is stretched by $\sqrt{2}$) (in 1D for illustration purpose).

Second, since the distances are invariant under the action of the affine group, we can set wlog. $N_1 = (0, I)$ (standard normal distribution) and let $N_2 = \text{diag}(u_1, \dots, u_d)$ where $u_i \sim \text{Unif}(0, a)$. As normals N_1 and N_2 separate to each others, we notice experimentally that the performance of the *cco* curve degrades in the second experiment with $a = 5$ (see Table 3): Indeed, the mixture geodesic works experimentally better than the C&O curve when $d \geq 11$.

Figure 9 and Figure 10 display the various curves considered for approximating the Fisher-Rao distance between bivariate normal distributions: For a curve $c(t)$, we visualize its corresponding

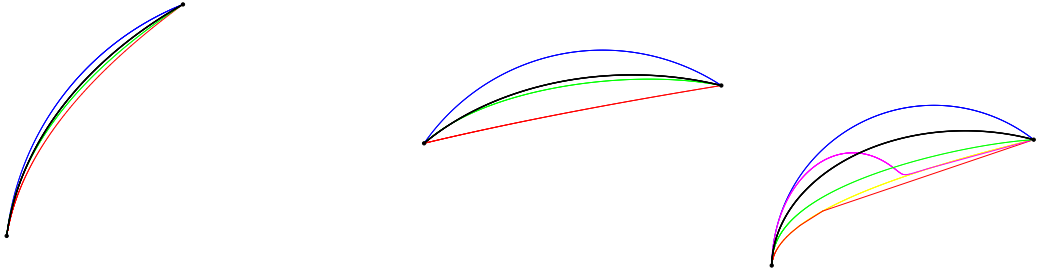


Figure 8: Visualizing the geodesics and curves in the Poincaré upper plane with x -axis stretched by $\sqrt{2}$: (a) and (b): Fisher-Rao geodesic (black), our projected Calvo & Oller curve (green), the mixture geodesic (blue), and the exponential geodesic (red). (c): interpolation in ordinary parameterization λ (yellow), mid mixture-exponential curve (purple). The range is $[-1, 1] \times (0, 2]$.

Table 3: Second set of experiments shows limitations of the $c_{\text{CO}}(t)$ curve.

d	κ_{CO}	κ_l	κ_e	κ_m
1	1.0569	1.1405	1.139	1.0734
5	1.1599	1.4696	1.5201	1.1819
10	1.2180	1.6963	1.7887	1.2184
11	1.2260	1.7333	1.8285	1.2235
12	1.2301	1.7568	1.8539	1.2282
15	1.2484	1.8403	1.9557	1.2367
20	1.2707	1.9519	2.0851	1.2466

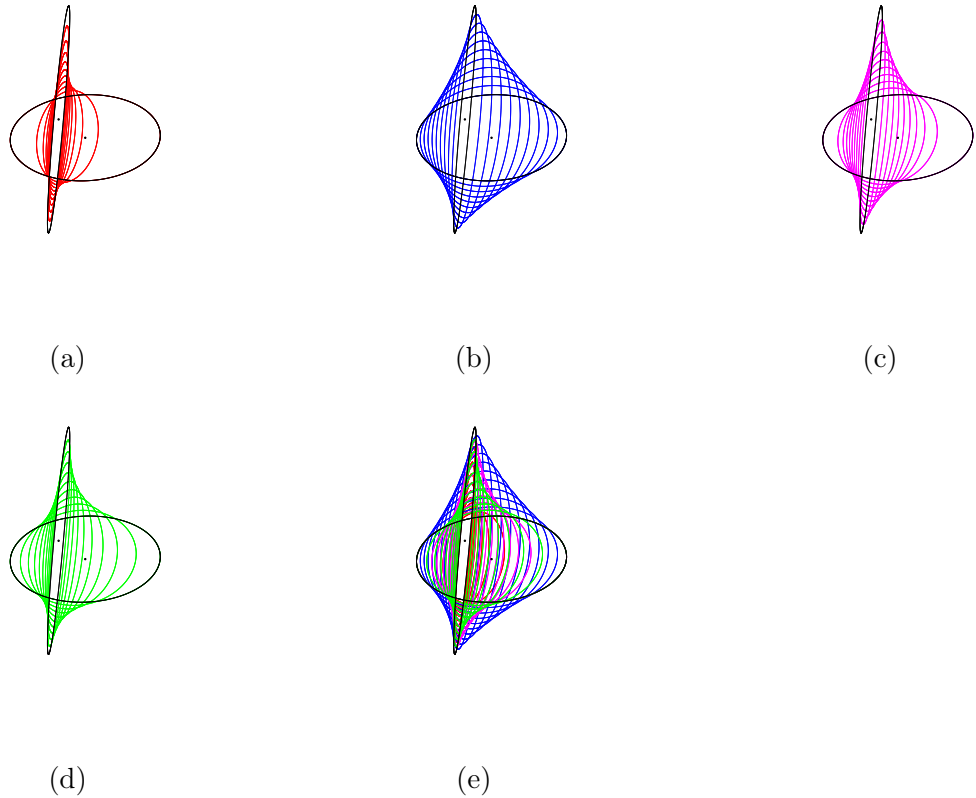


Figure 9: Visualizing at discrete positions (10 increment steps between 0 and 1) some curves used to approximate the Fisher-Rao distance between two bivariate normal distributions: (a) exponential geodesic $c^e = \gamma_{\mathcal{N}}^e$ (red), (b) mixture geodesic $c^m = \gamma_{\mathcal{N}}^m$ (blue), (c) mid mixture-exponential curve c^{em} (purple), (d) projected Calvo & Oller curve c^{CO} (green), and (e) All superposed curves at once.

bivariate normal distributions $(\mu_{c(t)}, \Sigma_{c(t)})$ at several increment steps $t \in [0, 1]$ by plotting the ellipsoid

$$E_{c(t)} = \mu_{c(t)} + \left\{ L^{\top} x, x = (\cos \theta, \sin \theta), \theta \in [0, 2\pi) \right\},$$

where $\Sigma_{c(t)} = L_{c(t)} L_{c(t)}^{\top}$.

Example 1 Let us report some numerical results for bivariate normals with $T = 1000$:

- We use the following example of Han and Park [15] (Eq. 26):

$$N_1 = \left(\begin{bmatrix} 0 \\ 0 \end{bmatrix}, \begin{bmatrix} 1 & 0 \\ 0 & 0.1 \end{bmatrix} \right), \quad N_2 = \left(\begin{bmatrix} 1 \\ 1 \end{bmatrix}, \begin{bmatrix} 0.1 & 0 \\ 0 & 1 \end{bmatrix} \right).$$

Their geodesic shooting algorithm [15] evaluates the Fisher-Rao distance to $\rho_{\mathcal{N}}(N_1, N_2) \approx \mathbf{3.1329}$ (precision 10^{-5}).

We get:

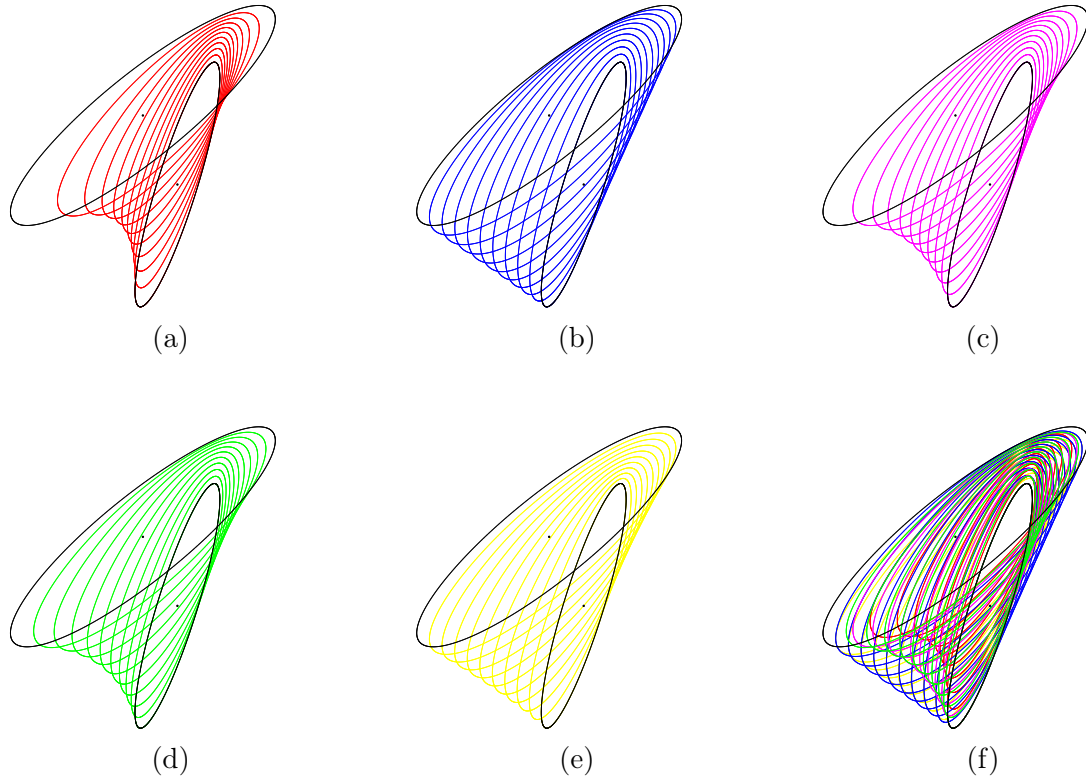


Figure 10: Visualizing at discrete positions (10 increment steps between 0 and 1) some curves used to approximate the Fisher-Rao distance between two bivariate normal distributions: (a) exponential geodesic $c^e = \gamma_{\mathcal{N}}^e$ (red), (b) mixture geodesic $c^m = \gamma_{\mathcal{N}}^m$ (blue), (c) mid mixture-exponential curve c^{em} (purple), (d) projected Calvo & Oller curve c^{CO} (green), (e) c^λ : ordinary linear interpolation in λ (yellow), and (f) All superposed curves at once.

- *Calvo & Oller lower bound*: $\rho_{\text{CO}}(N_1, N_2) \approx \mathbf{3.0470}$,
- *SPC upper bound* (Eq. 6): $U_{\text{SPC}}(N_1, N_2) \approx 5.4302$,
- $\sqrt{D_J}$ *upper bound*: $U_{\sqrt{J}}(N_1, N_2) \approx \mathbf{4.3704}$,
- $\tilde{\rho}_{\mathcal{N}}^{\lambda}(N_1, N_2) \approx 3.4496$,
- $\tilde{\rho}_{\mathcal{N}}^m(N_1, N_2) \approx 3.5775$,
- $\tilde{\rho}_{\mathcal{N}}^e(N_1, N_2) \approx 3.7314$,
- $\tilde{\rho}_{\mathcal{N}}^{\text{em}}(N_1, N_2) \approx 3.1672$,
- $\tilde{\rho}_{\mathcal{N}}^{\text{CO}}(N_1, N_2) \approx \mathbf{3.1391}$.

In that setting, the $\sqrt{D_J}$ upper bound is better than the upper bound of Eq. 6, and the projected Calvo & Oller geodesic yields the best approximation of the Fisher-Rao distance (Figure 11) with an absolute error of 0.0062 (about 0.2% relative error). When $T = 10$, we have $\tilde{\rho}_{\mathcal{N}}^{\text{CO}}(N_1, N_2) \approx 3.1530$, when $T = 100$, we get $\tilde{\rho}_{\mathcal{N}}^{\text{CO}}(N_1, N_2) \approx 3.1136$, and when $T = 500$ we obtain $\tilde{\rho}_{\mathcal{N}}^{\text{CO}}(N_1, N_2) \approx 3.1362$ (which is better than the approximation obtained for $T = 1000$). Figure 12 shows the fluctuations of the approximation of the Fisher-Rao distance by the projected C&O curve when T ranges from 3 to 100.

- Bivariate normal $N_1 = (0, I)$ and bivariate normal $N_2 = (\mu_2, \Sigma_2)$ with $\mu_2 = [10]^\top$ and $\Sigma_2 = \begin{bmatrix} 1 & -1 \\ -1 & 2 \end{bmatrix}$. We get
 - *Calvo & Oller lower bound*: 1.4498
 - *Upper bound of Eq. 6*: 2.6072
 - $\sqrt{D_J}$ *upper bound*: 1.5811
 - $\tilde{\rho}^{\lambda}$: 1.5068
 - $\tilde{\rho}^m$: 1.5320
 - $\tilde{\rho}^e$: 1.5456
 - $\tilde{\rho}^{\text{em}}$: 1.4681
 - $\tilde{\rho}^{\text{co}}$: 1.4673
- Bivariate normal $N_1 = (0, I)$ and bivariate normal $N_2 = (\mu_2, \Sigma_2)$ with $\mu_2 = [50]^\top$ and $\Sigma_2 = \begin{bmatrix} 1 & -1 \\ -1 & 2 \end{bmatrix}$. We get
 - *Calvo & Oller lower bound*: 3.6852
 - *Upper bound of Eq. 6*: 6.0392
 - $\sqrt{D_J}$ *upper bound*: 6.2048
 - $\tilde{\rho}^{\lambda}$: 5.7319
 - $\tilde{\rho}^m$: 4.4039
 - $\tilde{\rho}^e$: 5.9205
 - $\tilde{\rho}^{\text{em}}$: 4.2901
 - $\tilde{\rho}^{\text{co}}$: 4.3786

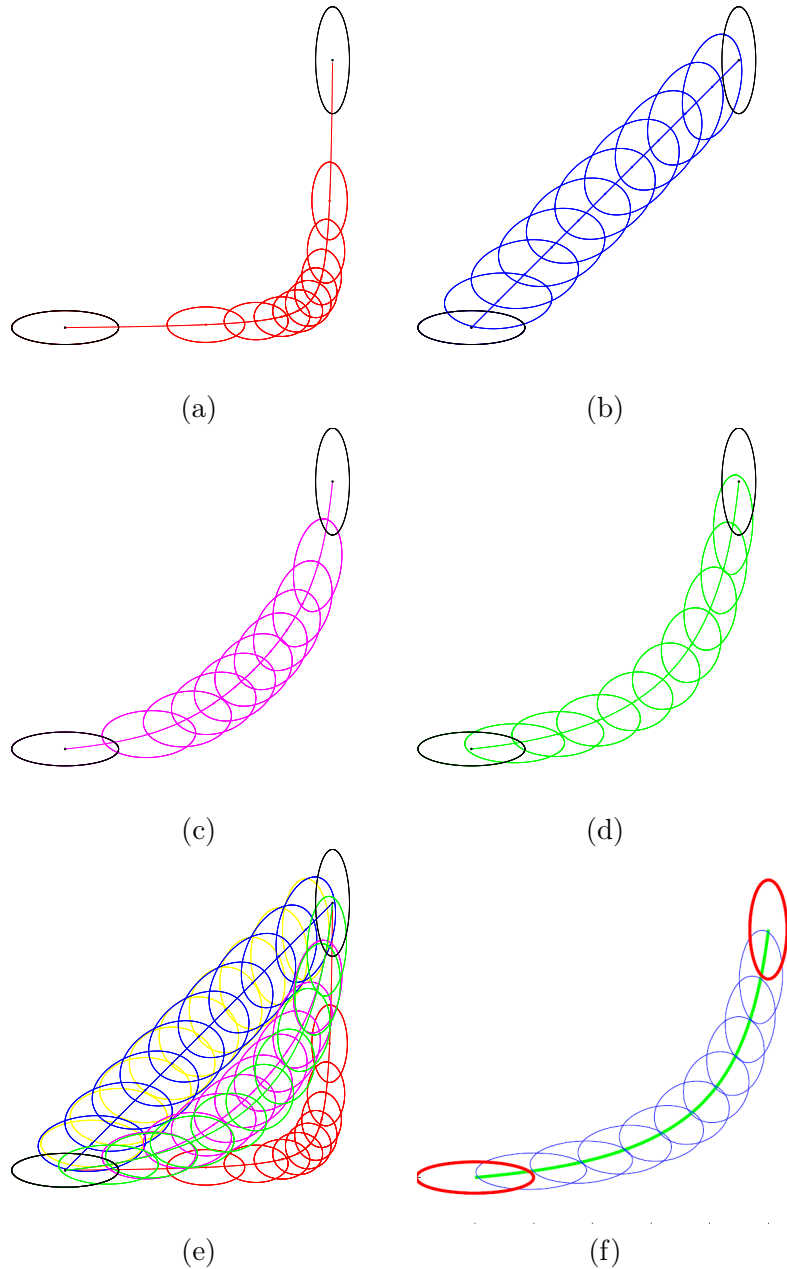


Figure 11: Comparison of our approximation curves with the Fisher-Rao geodesic (f) obtained by geodesic shooting (Figure 5 of [15]). Exponential (a) and mixture (b) geodesics with the mid exponential-mixture curve (c), and the projected C&O curve (d). Superposed curves (e) and comparison with geodesic shooting (Figure 5 of [15]). Beware that color coding are not related between (a) and (b), and scale for depicting ellipsoids are different.

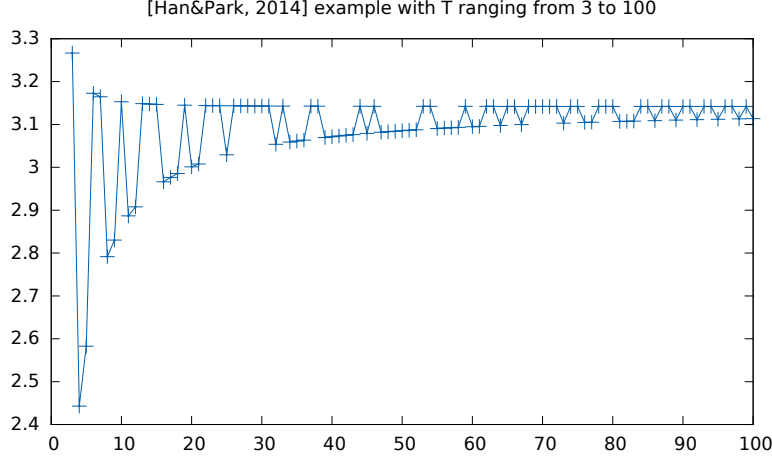


Figure 12: Approximating of the Fisher-Rao distance obtained by using the projected C&O curve when T ranges from 3 to 100.

4 Information-geometric properties of the embedding

In information geometry [1], the manifold \mathcal{N} admits a dual structure $(\mathcal{N}, g_{\mathcal{N}}^{\text{Fisher}}, \nabla_{\mathcal{N}}^e, \nabla_{\mathcal{N}}^m)$ when equipped with the exponential connection $\nabla_{\mathcal{N}}^e$ and the mixture connection $\nabla_{\mathcal{N}}^m$. The connections $\nabla_{\mathcal{N}}^e$ and $\nabla_{\mathcal{N}}^m$ are said dual since $\frac{\nabla_{\mathcal{N}}^e + \nabla_{\mathcal{N}}^m}{2} = \bar{\nabla}_{\mathcal{N}}$, the Levi-Civita connection induced by $g_{\mathcal{N}}^{\text{Fisher}}$. Furthermore, by viewing \mathcal{N} as an exponential family $\{p_{\theta}\}$ with natural parameter $\theta = (\theta_v, \theta_M)$ (using the sufficient statistics [28] $(x, -xx^{\top})$), and taking the convex log-normalizer function $F_{\mathcal{N}}(\theta)$ of the normals, we can build a dually flat space [1] where the canonical divergence amounts to a Bregman divergence which coincides with the reverse Kullback-Leibler divergence (KLD). The Legendre duality

$$F^*(\eta) = \langle \nabla F(\theta), \eta \rangle - F(\nabla F(\theta))$$

(with $\langle (v_1, M_1), (v_2, M_2) \rangle = v_1^{\top} v_2 + \text{tr}(M_1 M_2)$) yields: $\theta = (\theta_v, \theta_M) = (\Sigma^{-1} \mu, \frac{1}{2} \Sigma^{-1})$,

$$F_{\mathcal{N}}(\theta) = \frac{1}{2} \left(d \log \pi - \log |\theta_M| + \frac{1}{2} \theta_v^{\top} \theta_M^{-1} \theta_v \right),$$

$$\eta = (\eta_v, \eta_M) = \nabla F_{\mathcal{N}}(\theta) = \left(\frac{1}{2} \theta_M^{-1} \theta_v, \theta_M^{-1} \right),$$

$$F_{\mathcal{N}}^*(\eta) = -\frac{1}{2} \left(\log(1 + \eta_v^{\top} \eta_M^{-1} \eta_v) + \log |\eta_M| + d(\log 2\pi e) \right),$$

and we have

$$B_{F_{\mathcal{N}}}(\theta_1, \theta_2) = D_{\text{KL}}^*(p_{\lambda_1} : p_{\lambda_2}) = D_{\text{KL}}(p_{\lambda_2} : p_{\lambda_1}) = B_{F_{\mathcal{N}}^*}(\eta_2 : \eta_1),$$

where $D_{\text{KL}}^*[p : q] = D_{\text{KL}}[q : p]$ is the reverse KLD.

In a dually flat space, we can express the canonical divergence as a Fenchel-Young divergence using the mixed coordinate systems $B_{F_{\mathcal{N}}}(\theta_1 : \theta_2) = Y_{F_{\mathcal{N}}}(\theta_1 : \eta_2)$ where $\eta_i = \nabla F_{\mathcal{N}}(\theta_i)$ and

$$Y_{F_{\mathcal{N}}}(\theta_1 : \eta_2) := F_{\mathcal{N}}(\theta_1) + F_{\mathcal{N}}^*(\eta_2) - \langle \theta_1, \eta_2 \rangle.$$

The moment η -parameterization of a normal is $(\eta = \mu, H = -\Sigma - \mu\mu^\top)$ with its reciprocal function $(\lambda = \eta, \Lambda = -H - \eta\eta^\top)$.

Let $F_{\mathcal{P}}(P) = F_{\mathcal{N}}(0, P)$, $\bar{\theta} = \frac{1}{2}\bar{P}^{-1}$, $\bar{\eta} = \nabla F_{\mathcal{P}}(\bar{\theta})$. Then we have the following proposition which proves that the Fenchel-Young divergences in \mathcal{N} and $\overline{\mathcal{N}}$ (as a submanifold of \mathcal{P}) coincide:

Proposition 3 *We have*

$$\begin{aligned} D_{\text{KL}}[p_{\mu_1, \Sigma_1} : p_{\mu_2, \Sigma_2}] &= B_{F_{\mathcal{N}}}(\theta_2 : \theta_1) = Y_{F_{\mathcal{N}}}(\theta_2 : \eta_1) = Y_{F_{\mathcal{P}}}(\bar{\theta}_2 : \bar{\eta}_1) \\ &= B_{F_{\mathcal{P}}}(\bar{\theta}_2 : \bar{\theta}_1) = D_{\text{KL}}[p_{0, \bar{P}_1 = f(\mu_1, \Sigma_1)} : p_{0, \bar{P}_2 = f(\mu_2, \Sigma_2)}]. \end{aligned}$$

Consider now the ∇^e -geodesics and ∇^m -geodesics on \mathcal{N} (linear interpolation with respect to natural and dual moment parameterizations, respectively): $\gamma_{\mathcal{N}}^e(N_1, N_2; t) = (\mu_t^e, \Sigma_t^e)$ and $\gamma_{\mathcal{N}}^m(N_1, N_2; t) = (\mu_t^m, \Sigma_t^m)$.

Proposition 4 *The mixture geodesics are preserved by the embedding f : $f(\gamma_{\mathcal{N}}^m(N_1, N_2; t)) = \gamma_{\mathcal{P}}^m(f(N_1), f(N_2); t)$. The exponential geodesics are preserved for subspace of \mathcal{N} with fixed mean μ : \mathcal{N}_μ .*

Proof: For the m -geodesics, let us check that

$$f(\mu_t^m, \Sigma_t^m) = \begin{bmatrix} \Sigma_t^m + \mu_t \mu_t^{m\top} & \mu_t^m \\ \mu_t^m & 1 \end{bmatrix} = t \underbrace{f(\mu_1, \Sigma_1)}_{\bar{P}_1} + (1-t) \underbrace{f(\mu_2, \Sigma_2)}_{\bar{P}_2},$$

since $\Sigma_t^m + \mu_t \mu_t^{m\top} = \bar{\Sigma}_t + t\mu_1 \mu_1^\top + (1-t)\mu_2 \mu_2^\top = t(\Sigma_1 + \mu_1 \mu_1^\top) + (1-t)(\Sigma_2 + \mu_2 \mu_2^\top)$. Thus we have $f(\gamma_{\mathcal{N}}^m(N_1, N_2; t)) = \gamma_{\mathcal{P}}^m(\bar{P}_1, \bar{P}_2; t)$. \square

Therefore all algorithms on \mathcal{N} which only require m -geodesics or m -projections [1] by minimizing the right-hand side of the KLD can be implemented by algorithms on \mathcal{P} . See for example, the minimum enclosing ball approximation algorithm called BBC in [30]. Notice that $\overline{\mathcal{N}}_\mu$ (fixed mean normal submanifolds) preserve both mixture and exponential geodesics: The submanifolds $\overline{\mathcal{N}}_\mu$ are said doubly auto-parallel [31].

5 Conclusion and discussion

The Fisher-Rao distance between multivariate normals is not known in closed form. It is thus usually approximated by costly geodesic shooting techniques [15, 33, 4] in practice. In this work, we consider an alternative approach of approximating the Fisher-Rao distance by approximating the Riemannian lengths of closed-form curves. In particular, we considered the mixed exponential-mixture curved and the projected symmetric positive-definite matrix geodesic obtained from Calvo & Oller isometric SPD submanifold embedding [6]. We also reported a fast to compute simplex square root of Jeffreys' divergence for the Fisher-Rao distance which beats the upper bound of [39] when normal distributions are not too far from each others. Finally, we shows that not only Calvo & Oller SPD submanifold embedding [6] is isometric, it also preserves the Kullback-Leibler divergence, the Fenchel-Young divergence and the mixture geodesics.

Acknowledgments. I warmly thank Frédéric Barbaresco (Thales) and Mohammad Emtiyaz Khan (Riken AIP) for fruitful discussions about this work.

References

- [1] Shun-ichi Amari. *Information Geometry and Its Applications*. Applied Mathematical Sciences. Springer Japan, 2016.
- [2] Marc Arnaudon and Frank Nielsen. On approximating the Riemannian 1-center. *Computational Geometry*, 46(1):93–104, 2013.
- [3] Colin Atkinson and Ann FS Mitchell. Rao’s distance measure. *Sankhyā: The Indian Journal of Statistics, Series A*, pages 345–365, 1981.
- [4] Frédéric Barbaresco. Souriau exponential map algorithm for machine learning on matrix Lie groups. In *Geometric Science of Information: 4th International Conference, GSI 2019, Toulouse, France, August 27–29, 2019, Proceedings 4*, pages 85–95. Springer, 2019.
- [5] Martin Bauer, Martins Bruveris, and Peter W Michor. Uniqueness of the Fisher–Rao metric on the space of smooth densities. *Bulletin of the London Mathematical Society*, 48(3):499–506, 2016.
- [6] Miquel Calvo and Josep M Oller. A distance between multivariate normal distributions based in an embedding into the Siegel group. *Journal of multivariate analysis*, 35(2):223–242, 1990.
- [7] Miquel Calvo and Josep M Oller. A distance between elliptical distributions based in an embedding into the Siegel group. *Journal of Computational and Applied Mathematics*, 145(2):319–334, 2002.
- [8] Miquel Calvo and Josep Maria Oller. An explicit solution of information geodesic equations for the multivariate normal model. *Statistics & Risk Modeling*, 9(1-2):119–138, 1991.
- [9] Nikolai Nikolaevich Cencov. *Statistical decision rules and optimal inference*. Number 53. American Mathematical Soc., 2000.
- [10] Xiangbing Chen, Jie Zhou, and Sanfeng Hu. Upper bounds for Rao distance on the manifold of multivariate elliptical distributions. *Automatica*, 129:109604, 2021.
- [11] Jason Davis and Inderjit Dhillon. Differential entropic clustering of multivariate Gaussians. *Advances in Neural Information Processing Systems*, 19, 2006.
- [12] PS Eriksen. *Geodesics connected with the fischer metric on the multivariate normal manifold*. Institute of Electronic Systems, Aalborg University Centre, 1986.
- [13] Akio Fujiwara. Hommage to Chentsov’s theorem. *Information Geometry*, pages 1–20, 2022.
- [14] Wolfgang Globke and Raul Quiroga-Barranco. Information geometry and asymptotic geodesics on the space of normal distributions. *Information Geometry*, 4(1):131–153, 2021.
- [15] Minyeon Han and Frank C Park. DTI segmentation and fiber tracking using metrics on multivariate normal distributions. *Journal of mathematical imaging and vision*, 49:317–334, 2014.
- [16] Harold Hotelling. Spaces of statistical parameters. *Bull. Amer. Math. Soc*, 36:191, 1930.

[17] Takuro Imai, Akira Takaesu, and Masato Wakayama. Remarks on geodesics for multivariate normal models. 2011.

[18] Hiroto Inoue. Group theoretical study on geodesics for the elliptical models. In *Geometric Science of Information: Second International Conference, GSI 2015, Palaiseau, France, October 28-30, 2015, Proceedings 2*, pages 605–614. Springer, 2015.

[19] A. T. James. The variance information manifold and the functions on it. In *Multivariate Analysis-III*, pages 157–169. Elsevier, 1973.

[20] Peihua Li, Qilong Wang, Hui Zeng, and Lei Zhang. Local log-Euclidean multivariate Gaussian descriptor and its application to image classification. *IEEE transactions on pattern analysis and machine intelligence*, 39(4):803–817, 2016.

[21] Tengyuan Liang, Tomaso Poggio, Alexander Rakhlin, and James Stokes. Fisher-Rao metric, geometry, and complexity of neural networks. In *The 22nd international conference on artificial intelligence and statistics*, pages 888–896. PMLR, 2019.

[22] Miroslav Lovrić, Maung Min-Oo, and Ernst A Ruh. Multivariate normal distributions parametrized as a Riemannian symmetric space. *Journal of Multivariate Analysis*, 74(1):36–48, 2000.

[23] Charles A Micchelli and Lyle Noakes. Rao distances. *Journal of Multivariate Analysis*, 92(1):97–115, 2005.

[24] Maher Moakher and Mourad Zéraï. The Riemannian geometry of the space of positive-definite matrices and its application to the regularization of positive-definite matrix-valued data. *Journal of Mathematical Imaging and Vision*, 40(2):171–187, 2011.

[25] Pierre-Alexandre Murena, Antoine Cornuéjols, and Jean-Louis Désalles. Opening the parallelogram: Considerations on non-euclidean analogies. In *Case-Based Reasoning Research and Development: 26th International Conference, ICCBR 2018, Stockholm, Sweden, July 9-12, 2018, Proceedings 26*, pages 597–611. Springer, 2018.

[26] Xuan Son Nguyen. Geomnet: A neural network based on Riemannian geometries of SPD matrix space and Cholesky space for 3d skeleton-based interaction recognition. In *Proceedings of the IEEE/CVF International Conference on Computer Vision*, pages 13379–13389, 2021.

[27] Frank Nielsen. Cramér-Rao lower bound and information geometry. *Connected at Infinity II: A Selection of Mathematics by Indians*, pages 18–37, 2013.

[28] Frank Nielsen. On the Jensen–Shannon symmetrization of distances relying on abstract means. *Entropy*, 21(5):485, 2019.

[29] Frank Nielsen. The Siegel–Klein Disk: Hilbert Geometry of the Siegel Disk Domain. *Entropy*, 22(9):1019, 2020.

[30] Richard Nock and Frank Nielsen. Fitting the smallest enclosing Bregman ball. In *Machine Learning: ECML 2005: 16th European Conference on Machine Learning, Porto, Portugal, October 3-7, 2005. Proceedings 16*, pages 649–656. Springer, 2005.

[31] Atsumi Ohara. Doubly autoparallel structure on positive definite matrices and its applications. In *International Conference on Geometric Science of Information*, pages 251–260. Springer, 2019.

[32] Marine Picot, Francisco Messina, Malik Boudiaf, Fabrice Labeau, Ismail Ben Ayed, and Pablo Piantanida. Adversarial robustness via Fisher-Rao regularization. *IEEE Transactions on Pattern Analysis and Machine Intelligence*, 2022.

[33] Marion Pilté and Frédéric Barbaresco. Tracking quality monitoring based on information geometry and geodesic shooting. In *2016 17th International Radar Symposium (IRS)*, pages 1–6. IEEE, 2016.

[34] Julianna Pinele, João E Strapasson, and Sueli IR Costa. The Fisher–Rao distance between multivariate normal distributions: Special cases, bounds and applications. *Entropy*, 22(4):404, 2020.

[35] Branislav Popović, Marko Janev, Lidija Krstanović, Nikola Simić, and Vlado Delić. Measure of Similarity between GMMs Based on Geometry-Aware Dimensionality Reduction. *Mathematics*, 11(1):175, 2022.

[36] C Radhakrishna Rao. Information and accuracy attainable in the estimation of statistical parameters. *Bulletin of the Calcutta Mathematical Society*, 37(3):81–91, 1945.

[37] Carl Ludwig Siegel. *Symplectic geometry*. Elsevier, 2014. first printed in 1964.

[38] Lene Theil Skovgaard. A Riemannian geometry of the multivariate normal model. *Scandinavian journal of statistics*, pages 211–223, 1984.

[39] João E Strapasson, Julianna PS Porto, and Sueli IR Costa. On bounds for the Fisher-Rao distance between multivariate normal distributions. In *AIP Conference Proceedings*, volume 1641, pages 313–320. American Institute of Physics, 2015.

[40] Mengjiao Tang, Yao Rong, Jie Zhou, and X Rong Li. Information geometric approach to multisensor estimation fusion. *IEEE Transactions on Signal Processing*, 67(2):279–292, 2018.

[41] Geert Verdoolaege. A new robust regression method based on minimization of geodesic distances on a probabilistic manifold: Application to power laws. *Entropy*, 17(7):4602–4626, 2015.

[42] Geert Verdoolaege and Paul Scheunders. On the geometry of multivariate generalized Gaussian models. *Journal of mathematical imaging and vision*, 43:180–193, 2012.

[43] Qilong Wang, Peihua Li, and Lei Zhang. G2denet: Global gaussian distribution embedding network and its application to visual recognition. In *Proceedings of the IEEE conference on computer vision and pattern recognition*, pages 2730–2739, 2017.

[44] Wen Wang, Ruiping Wang, Zhiwu Huang, Shiguang Shan, and Xilin Chen. Discriminant analysis on Riemannian manifold of Gaussian distributions for face recognition with image sets. In *Proceedings of the IEEE conference on computer vision and pattern recognition*, pages 2048–2057, 2015.

[45] Joseph Wells, Mary Cook, Karleigh Pine, and Benjamin D Robinson. Fisher-Rao distance on the covariance cone. *arXiv preprint arXiv:2010.15861*, 2020.

A Embedding multivariate normals on the Siegel upper space

The Siegel upper space is the space of symmetric complex matrices with imaginary positive-definite matrices [37, 29]:

$$\mathbb{SH}(d) := \{Z = X + iY : X \in \text{Sym}(d), Y \in \mathcal{P}(d)\}, \quad (7)$$

where $\text{Sym}(d)$ is the space of symmetric real $d \times d$ matrices. The Siegel infinitesimal square line element is

$$ds_{\mathbb{SH}}^2(Z) = 2\text{tr}(Y^{-1}dZ Y^{-1}d\bar{Z}). \quad (8)$$

When $Z = iY$, we have $dZ = idY$, $d\bar{Z} = -idY$, and

$$ds_{\mathbb{SH}}^2(iY) = 2\text{tr}((Y^{-1}dY)^2).$$

That is, four times the square length of the Fisher matrix of centered normal distributions $ds_P^2 = \frac{1}{2}\text{tr}((P^{-1}dP)^2)$.

The Siegel distance between Z_1 and $Z_2 \in \mathbb{SH}(d)$ is

$$\rho_{\mathbb{SH}}(Z_1, Z_2) = \sqrt{\sum_{i=1}^d \log^2 \left(\frac{1 + \sqrt{r_i}}{1 - \sqrt{r_i}} \right)}, \quad (9)$$

where

$$r_i = \lambda_i(R(Z_1, Z_2)), \quad (10)$$

with $R(Z_1, Z_2)$ denoting the matrix generalization of the cross-ratio:

$$R(Z_1, Z_2) := (Z_1 - Z_2)(Z_1 - \bar{Z}_2)^{-1}(\bar{Z}_1 - \bar{Z}_2)(\bar{Z}_1 - Z_2)^{-1}, \quad (11)$$

and $\lambda_i(M)$ denotes the i -th largest (real) eigenvalue of (complex) matrix M .

We can embed a multivariate normal $N = (\mu, \Sigma)$ into $\mathbb{SH}(d)$ as follows:

$$N = (\mu, \Sigma) \rightarrow Z(N) := (\mu\mu^\top + i\Sigma),$$

and consider the Siegel distance on the embedded normal distributions as another distance between multivariate normals:

$$\rho_{\mathbb{SH}}(N_1, N_2) = \rho_{\mathbb{SH}}(Z(N_1), Z(N_2)). \quad (12)$$

Notice that the real matrix part of the $Z(N)$'s are all of rank one.